Research Square

Preprints are preliminary reports that have not undergone peer review.
They should not be considered conclusive, used to inform clinical practice,
or referenced by the media as validated information.

Fabrication of Waterborne Polyurethane Flexible Strain Sensors Based on KH560-MXene/MWCNTs Synergistic Effects and the Application in Motion Posture Monitoring

Xunlong Wang
Qingdao Marine Comprehensive Proving Ground Co., Ltd
Peng Shi
Qingdao Marine Comprehensive Proving Ground Co., Ltd
Zhaoliang Li
Qingdao Marine Comprehensive Proving Ground Co., Ltd
Shuyou Liu
Qingdao Marine Comprehensive Proving Ground Co., Ltd
Qing Liu
Qingdao Marine Comprehensive Proving Ground Co., Ltd
Ying Chen
cy_198812@163.com

Qingdao Marine Comprehensive Proving Ground Co., Ltd

Research Article

Keywords: Flexible strain sensors, MXene, Carbon nanotubes, Density functional theory, Composite conductive network

Posted Date: November 13th, 2026

DOI: https://doi.org/10.21203/rs.3.rs-11510771/v1

License: This work is licensed under a Creative Commons Attribution 4.0 International License.
Read Full License

Additional Declarations: No competing interests reported.

Fabrication of Waterborne Polyurethane Flexible Strain Sensors Based on KH560-MXene/MWCNTs Synergistic Effects and the Application in Motion Posture Monitoring

Xunlong Wang[1], Peng Shi[1], Zhaoliang Li[1], Shuyou Liu[1], Qing Liu[1], Ying Chen[1]*

(1 Qingdao Marine Comprehensive Proving Ground Co., Ltd, 266237, Qingdao, China.)

* Corresponding authors (E-mails: cy_198812@163.com (Ying Chen).

Abstract

Flexible sensors serve as the core component of wearable electronics and intelligent health monitoring devices, possessing enormous application potential in the fields of human physiological signal acquisition and motion behavior detection. Nevertheless, flexible sensing materials generally suffer from poor environmental stability, weak anti-interference capability of sensing signals, and inevitable degradation of sensing performance during long-term cyclic operation, which severely restrict their large-scale practical applications. To address these issues, waterborne polyurethane (WPU) is adopted as the flexible matrix, modified MXene nanosheets with KH560 and multi-walled carbon nanotubes (MWCNTs) were introduced as hybrid conductive fillers. An integrated high-performance flexible strain sensor is fabricated via a solution blending and casting strategy. Through hydrogen bonding and electrostatic adsorption effects, a 1D-2D interconnected conductive network is constructed, where MXene acts as the primary conductive unit and MWCNTs function as interconnection bridging segments. This flexible sensor based on the composite system exhibits superior comprehensive performances, including a high gauge factor of 2.81, a broad strain detection range of 0-2800%, rapid response and recovery times of 150 ms and 120 ms, as well as excellent cycling stability over 3000 cycles. Density functional theory (DFT) calculations elucidate the interfacial mechanism of the MXene/MWCNTs heterojunction, verifying that the sensing mechanism originates from the synergistic effect of band structure evolution and conductive network reconstruction. Furthermore, the sensor enables real-time monitoring of electromyographic signals during human movements, demonstrating great application potential in intelligent wearable electronics.

Keywords： Flexible strain sensors; MXene; Carbon nanotubes; Density functional theory; Composite conductive network

1.Introduction

With the rapid development of the internet of things and artificial intelligence technologies[1], flexible sensors as core components of wearable electronic devices-have demonstrated immense application potential in fields such as human motion monitoring, telemedicine, human-computer interaction, and soft robotics[2]. Compared to traditional rigid strain sensors, flexible strain sensors offer unique advantages such as lightweight design, stretchability, and skin-adhesive properties. They can adapt to the deformation requirements of the human body's complex surfaces[3], effectively addressing the shortcomings of traditional rigid sensors, such as poor adhesion, inability to accommodate large-angle joint movements and low wearing comfort. As a result, they have become the core supporting devices for the precise monitoring of human movement and posture, driving the evolution of motion monitoring from coarse sensing to precise quantification. Among various sensing devices, resistive flexible strain sensors have attracted extensive research attention and practical applications owing to their superiorities including structural simplicity and stable signal output. Typically, such sensors are fabricated by compounding conductive nanofillers with flexible polymer matrices, which can construct conductive pathways inside the matrix that enable synchronous deformation with the substrate[4-6]. Nevertheless, critical challenges still remain in the further development of these sensors: it is difficult to achieve favorable sensitivity within an effective strain range, while the conductive network is prone to irreversible structural damage under long-term cyclic loading. To address the above bottlenecks, modification strategies such as hierarchical structure regulation of conductive networks, hybrid compounding of conductive fillers, interfacial reinforcement of two-phase components, and introduction of self-healing functions can be adopted to synergistically enhance the comprehensive sensing performance. These optimization approaches have become the mainstream research focus and development trend in the field of flexible strain sensors[7-10].

At present, the application of composite conductive fillers has become prevalent in the research of flexible sensors. According to the geometric dimensions of materials, composite fillers can be classified into zero-dimensional nanoparticles, one-dimensional nanowires, two-dimensional nanosheets, and multidimensional hybrid systems. For example, zero-dimensional carbon black and metal nanoparticles feature facile synthesis and favorable dispersion, yet their high percolation threshold and point-contact conduction characteristics inevitably restrict the sensing efficiency. One-

dimensional carbon nanotubes[11] and silver nanowires possess an ultra-high aspect ratio, which facilitates the construction of long-range conductive pathways with a low percolation threshold. Nevertheless, issues such as entanglement, agglomeration and corrosion failure remain to be addressed. Two-dimensional graphene provide abundant force-sensitive contact sites owing to their ultra-large specific surface area[12], while interlayer stacking and oxidation inevitably reduce the effective sensing area. To break through the inherent bottlenecks of single-dimensional fillers, the hybridization of fillers with distinct geometric characteristics to construct a multidimensional interpenetrating conductive network has emerged as a mainstream strategy to achieve leapfrog improvement in sensing performance[13].

Two-dimensional transition metal carbides/nitrides (MXene)[14-15] have emerged as highly popular materials in the field of flexible sensors owing to their metal-like electrical conductivity (up to 10^4 $S \cdot cm^{-1}$), abundant surface functional groups (-O, -F, -OH), and excellent hydrophilicity. Nevertheless, pure MXene networks are prone to irreversible interlayer slippage and large-scale delamination under tensile strain, which triggers catastrophic fracture of conductive pathways and restricts the sensing detection range to a small strain region[16]. To address this issue, one-dimensional multi-walled carbon nanotubes (MWCNTs) with ultra-high aspect ratio and superior mechanical flexibility are introduced as conductive nanobridges to effectively interconnect adjacent MXene conductive islands, constructing a cross-scale interconnected synergistic percolation network. Under tensile deformation, even if remarkable relative slippage occurs between MXene nanosheets, the highly flexible MWCNTs can maintain electron transport through self-entanglement, stretching and axial slippage, thereby preventing the complete rupture of conductive pathways. More importantly, the high elastic resilience and mechanical dissipation capability of MWCNTs can efficiently dissipate strain energy and restrain the irreversible aggregation and permanent structural damage of MXene layers. Upon stress release, the traction effect of the "nanobridge" enables the reconstruction of conductive paths for slipped nanosheets, which significantly reduces signal drift and hysteresis, and endows the sensor with stable signal transmission capability after thousands of cycles. Furthermore, non-covalent interfacial interactions such as hydrogen bonds formed between polar terminal groups on the surface of MXene and defect sites or modified groups on MWCNT walls not only enhance stress transfer efficiency and network structural integrity, but also further synergistically optimize the strain tolerance and dynamic durability of the sensor. By

combining two-dimensional MXene with one-dimensional multi-walled carbon nanotubes, it is possible to achieve high sensitivity, a wide detection range, and excellent cycling stability in a synergistic manner[17-18].

In the field of flexible sensing composite systems, adopted flexible matrix materials primarily include polydimethylsiloxane (PDMS), polyimide (PI), Ecoflex elastomer and polyurethane (PU)[19-20]. Among them, PDMS exhibits favorable flexibility and biocompatibility, but it possesses an inherently inert surface with weak interfacial adhesion to MXene and carbon nanotubes. Under large strain, conductive fillers are prone to slippage and detachment, resulting in severe signal drift and inferior cycling durability. PI delivers exceptional thermal and chemical stability, whereas its high rigidity and low elongation at break limit its applicability in large-deformation flexible sensing; additionally, it suffers from high cost and complicated fabrication procedures[21-23]. Ecoflex elastomer features an ultra-low modulus and superior stretchability, but it is compromised by insufficient mechanical strength, poor thermal resistance, and weak interfacial bonding, inevitably leading to structural fatigue and signal instability under long-term cyclic loading. In contrast, waterborne polyurethane (WPU) possesses a unique microphase-separated structure of soft and hard segments, integrating excellent stretchability, elastic resilience, and mechanical stability. Abundant polar groups on the WPU molecular chains can form hydrogen bonds and other non-covalent interfacial interactions with oxygen-containing functional groups on MXene surfaces and defect sites of carbon nanotubes, effectively improving the interfacial compatibility and stress transfer efficiency between fillers and the matrix[23-26]. This structure restricts the interlayer slippage of MXene nanosheets and maintains the structural integrity of the conductive network. Moreover, WPU exhibits excellent film-forming performance, environmental friendliness, low toxicity, facile processing capability and superior environmental adaptability, making it highly suitable for wearable flexible electronics applications. By comprehensively comparing the mechanical properties, interfacial bonding capability, processability and long-term stability of various flexible matrices, WPU is ultimately selected as the flexible substrate in this work to construct MXene/MWCNTs/WPU flexible sensors[27-28].

In this work, waterborne polyurethane (WPU) is adopted as a flexible matrix, and MXene nanosheets combined with MWCNTs are employed as hybrid conductive fillers to fabricate high-performance flexible strain-sensing composites. By tuning the filler ratio of MXene to MWCNTs, the internal conductive network is rationally optimized.

The as-fabricated strain sensor delivers outstanding comprehensive sensing performances, including a gauge factor of 2.81, an ultra-broad working strain range of 0-2800%, and superior cycling durability over 3000 loading-unloading cycles. Based on density functional theory (DFT) calculations[29], the electronic configuration and interfacial charge transport behavior of MXene/MWCNTs heterojunctions are systematically unraveled, which clarifies the underlying microscopic mechanism responsible for the synergistic enhancement in sensing performance originating from binary fillers. This study provides solid experimental foundations and theoretical guidelines for the structural design and performance optimization of advanced flexible strain sensors.

2. Experimental Section

2.1 Materials

MAX phase precursor (Ti_3AlC_2, purity > 98%, 400 mesh) was purchased from Jilin 11 Technology Co., Ltd. Lithium fluoride (LiF, purity 99.9%) and hydrochloric acid (HCl, 30wt%) were supplied by Sinopharm Chemical Reagent Co., Ltd. Carboxylated multi-walled carbon nanotubes (MWCNTs-COOH) with an outer diameter of 10-20 nm, length of 5-15 μm and purity over 95% were obtained from Nanjing XFNANO Materials Tech Co., Ltd. 3-Glycidoxypropyltrimethoxysilane (KH560) and waterborne polyurethane (WPU, 30 wt%, molecular weight: approximately 50,000) were provided by Bayer AG, Germany. Deionized water was used throughout the entire experiment.

2.2 Synthesis of MXene Nanosheets

MXene nanosheets were prepared via an in-situ etching method using LiF/HCl mixed solution. Firstly, 1.6 g of LiF was dissolved in 20 mL of 9 M HCl solution under magnetic stirring for 30 min to achieve complete dissolution. Subsequently, 1.0 g of MAX phase powder was slowly added into the above solution, and the reaction was carried out at 35 °C under continuous stirring for 24 h. After the reaction was completed, the resultant mixture was centrifuged at 3500 rpm for 30 min. The supernatant was discarded, and the sediment was redispersed in deionized water. The washing and centrifugation process was repeated until the pH value of the supernatant approached approximately 6. Afterwards, the precipitate was dispersed in 100 mL of deionized water and ultrasonically treated for 2 h under argon atmosphere protection to achieve delamination of MXene. Finally, the mixture was centrifuged at 3500 rpm for 30 min, and the upper dark green suspension was collected, which was the few layer MXene

nanosheet dispersion. The few layer MXene nanosheet powder was obtained after vacuum freeze-drying for 48 h.

2.3 Preparation of KH560/MXene/MWCNTs/WPU flexible strain sensors

MXene powder and MWCNTs powder were mixed at a mass ratio of 2:1 with varying MXene contents, followed by the addition of a small amount of KH560. The resultant mixture was then added into 20 mL WPU emulsion. The mixture was continuously stirred for 2 h until homogeneous. The obtained homogeneous mixture was poured into a polytetrafluoroethylene (PTFE) mold and dried in an oven at 60 °C for 24 h to prepare MXene/MWCNTs/WPU composite films. The samples were labeled as d-MC_x/WPU (x = 0.5, 1, 2, 3) according to the added mass of MXene and MWCNTs. The thickness of each film was controlled at 150 μm. The films were cut into rectangular strips with a size of 40 × 5 mm. Copper foil electrodes were pasted at both ends of the strips using conductive silver adhesive to fabricate flexible strain sensors.

2.4 Characterization

Scanning electron microscopy (SEM, JEOL JSM-7800F) and transmission electron microscopy (TEM, JEOL JEM2100) were employed to characterize the micromorphology of MXene nanosheets, MWCNTs, and MC-WPU flexible sensors. X-ray diffraction (XRD, Bruker D8 Advance) was utilized to analyze the crystal structure of the materials, with a scanning range of 5°- 80° and a scanning rate of 2° min^{-1}. A TAQ600 thermogravimetric analyzer (TGA) is used to carry out thermal performance tests on MXene, and MXene/MWCNTs under a high-purity nitrogen protection atmosphere (flow rate 50 mL/min) at a heating rate of 10 ℃/min, and the range is 25-800 ℃/min, and the temperature range is 25-800℃. X-ray photoelectron spectroscopy (XPS, Thermo Scientific ESCALAB 250Xi) was adopted to investigate the surface functional groups of MXene/MWCNTs hybrids. Fourier transform infrared spectroscopy (FTIR, Thermo Nicolet iS50) was used to characterize the interfacial interaction between different fillers. The mechanical properties of the flexible sensors were tested at diverse stretching rates by a universal material testing machine (zhiqu990B).

2.5 Strain Sensing Performance Test

The sensing performance tests were conducted on a combined system consisting of a universal material testing machine and a Keithley 2450 source meter. The sensor was clamped onto the fixture of the testing machine, with its electrodes connected to the source meter. Under a constant bias voltage of 1 V, the real-time current variation

during the stretching-releasing process was recorded. The relative resistance change is defined as $\Delta R/ R_0= (R - R_0)/ R_0$, where R_0 represents the initial resistance and R denotes the real-time resistance during stretching. The gauge factor[29-32] (GF) is defined by the following formula:

$$GF = \frac{\Delta R / R_0}{\varepsilon} \quad (1)$$

The response time and recovery time are defined as the time required for the resistance variation to reach 10% of the stable value during the stretching and releasing processes, respectively. The limit of detection was determined via micro-step strain tests. The cyclic stability was evaluated by repeated stretching-releasing cycles at a tensile strain of 100%.

3. Results and Discussion

The preparation procedures of MXene, MXene/MWCNTs and d-MC_x/WPU flexible sensors are presented in Fig. 1(a-b). Firstly, using HCl to etch the MAX phase precursor to prepare MXene solution. Then, 1D carboxylated multi-walled carbon nanotubes (MWCNTs-COOH) are incorporated into the system. Their high electrical conductivity reduces the overall resistance of the conductive fillers, and the surface-grafted functional groups facilitate effective interfacial bonding with MXene. Subsequently, waterborne polyurethane (WPU) solution is added and thoroughly blended with the MXene/MWCNTs mixture to ensure homogeneous dispersion of the fillers. The d-MC_x/WPU flexible sensor is ultimately obtained through an integrated casting process. Fig. 1(c) illustrates the practical applications of the d-MC_x/WPU flexible sensor in human postures monitoring.

Fig2. (a) displays the typical layered stacking morphology of MXene after etching, verifying the successful exfoliation of MAX. The cross-sectional SEM morphologies of MXene/MWCNTs/WPU composite films with different filler concentrations are shown in Fig. 2(b-c). At low filler loading, the composite film exhibits a rough and discontinuous fracture surface, accompanied by numerous obvious cracks, voids, and phase separation, as well as distinct filler agglomeration regions. These observations indicate poor interfacial compatibility and weak interfacial adhesion between the MXene/MWCNTs fillers and the WPU matrix, along with defective crosslinking networks and low crosslinking density of the WPU matrix. Severe agglomeration of MXene sheets and MWCNTs disrupts the continuity of the polymer network, creating defect sites and stress concentration points that significantly compromise the structural

integrity of the composite film. In contrast, the composite film modified with KH560 and optimized filler concentration presents a dense and uniform cross-section, without obvious cracks, voids or phase boundaries. MXene and MWCNTs fillers are homogeneously dispersed and tightly encapsulated by the continuous WPU matrix, forming an integrated "conductive island-conductive bridge" network structure. These results demonstrate that the interfacial interaction and adhesion between the fillers and the matrix are significantly enhanced in the optimized system. The fillers are sufficiently wetted by the WPU resin, and possible hydrogen bonding between the functionalized fillers and polyurethane chains may be established. Meanwhile, the uniform filler distribution ensures the formation of a continuous, high-density crosslinking network of the WPU matrix, which effectively inhibits crack initiation and propagation. Consequently, the structural stability, mechanical properties, and functional characteristics such as electrical conductivity of the composite film are remarkably improved.

To investigate the thermal stability of MXene, MWCNTs and MXene/MWCNTs, TG analysis was employed to characterize the thermal decomposition behavior of the samples under a nitrogen atmosphere. And the corresponding results are presented in Fig. 2(d). Pure MXene exhibits excellent thermal stability from room temperature to 800 °C, with only a slight weight loss at low temperature attributed to the desorption of surface adsorbed water and a small amount of terminal hydroxyl groups, and its final residual mass reaches as high as 98.02%. In contrast, MWCNTs show a distinct multi-stage weight loss behavior. The weight loss at low temperatures is mainly ascribed to the removal of adsorbed water and oxygen-containing functional groups, while the continuous weight loss at moderate and high temperatures originates from the thermal decomposition of amorphous carbon and defective structures. The final residual mass was only 75.72%. This indicates that the oxygen-containing groups introduced by carboxylation modification remarkably reduce the thermal stability of MWCNTs. For the d-MXene/MWCNTs, its thermal decomposition behavior lies between those of the two individual components, having a final residual mass of 92.54%. Compared with MWCNTs, the composite exhibits a much slower weight loss rate and greatly improved thermal stability at moderate and high temperatures. This is attributed to the protective effect of the high thermal-resistant MXene skeleton on MWCNTs, as well as the suppression of the thermal decomposition of oxygen-containing functional groups by hydrogen bonding and other interfacial interactions. The above results confirm that the

combination of MXene and MWCNTs effectively improves the thermal stability of the single-component material.

The XRD patterns in the Fig.2(e) clearly demonstrate the phase and structural characteristics of MXene, multi-walled carbon nanotubes (MWCNTs), and the KH560-MXene/MWCNTs composite (d-MC). For pure MXene[33], a strong characteristic diffraction peak corresponding to the (002) plane appears at $2\theta = 9.6°$, which is associated with its typical layered structure. For pure MWCNTs, a broad characteristic peak of the graphitic carbon (002) plane is observed at approximately $2\theta = 25.8°$, accompanied by a secondary weak peak near $2\theta \approx 43°$, confirming its graphitic carbon structure and high purity. In contrast, for the MXene/MWCNTs composite (d-MC), the distinct (002) peak of MXene at ~10° disappears significantly, whereas the characteristic (002) peak of MWCNTs at ~26° is retained but exhibits reduced intensity and broadened peak shape. These changes directly verify that MWCNTs have successfully intercalated into and expanded the layered structure of MXene, disrupting the original periodic stacking of MXene nanosheets. Overall, these results confirm the effective integration of MXene and MWCNTs, forming a structure that suppresses the restacking of MXene layers, thereby improving ion transport efficiency and constructing an enhanced conductive network.

In Fig. 2(f), the FTIR spectrum of MWCNTs-COOH exhibits a characteristic -OH stretching vibration peak at 3660 cm^{-1}, along with C=O stretching and C=C skeletal vibration peaks of carbon nanotubes at 1580 cm^{-1} and 1350 cm^{-1} respectively, confirming that carboxylation modification successfully introduced reactive functional groups onto the MWCNTs surface. For the MXene spectrum, the absorption peak at 3439 cm^{-1} corresponds to the stretching vibration of surface -OH groups. For the MXene/MWCNTs composite, the spectrum inherits the characteristic signals of both components: it retains the -OH absorption peak of MXene while simultaneously displaying the C=O and C=C characteristic peaks of MWCNTs-COOH, directly verifying the coexistence of the two components in the composite system. Notably, the -OH peak at 3440 cm^{-1} in the composite is significantly intensified and broadened, indicating the formation of hydrogen-bonding interactions between the hydroxyl groups on MXene and the carboxyl groups of MWCNTs-COOH, which optimizes the interfacial interaction between the two materials. These results demonstrate that MXene and MWCNTs-COOH achieve effective hybridization via hydrogen bonding, providing

a structural improvement for constructing continuous and stable 1D-2D conductive network.

The full-range XPS survey spectrum in Fig. 3(a) displays distinct characteristic peaks assigned to C 1s, O 1s and Ti 2p core-level signals, verifying the successful incorporation of C, O and Ti elements within the as-prepared composite. High-resolution XPS spectra of individual elements are further deconvoluted to analyze interfacial chemical bonding. As presented in Fig. 3(b), the C 1s spectrum is split into two subpeaks centered at ~284.6 eV and ~282.2 eV, which correspond to C-C and C-Ti bonds, respectively. The C-C component originates from carbon nanotubes and intrinsic carbon skeletons of MXene nanosheets, while the C-Ti peak serves as a fingerprint of pristine MXene, demonstrating the well-preserved crystalline structure of MXene after composite fabrication. For the Ti 2p spectrum in Fig. 3(c), four fitted subpeaks are resolved, consisting of Ti-C $2p_{3/2}$, Ti-C $2p_{1/2}$, Ti-O $2p_{3/2}$ and Ti-O $2p_{1/2}$ signals. The Ti-C peaks derive from the inner skeletal bonding of MXene, whereas Ti–O bonds stem from oxygen-containing terminal groups anchored on MXene surfaces; these polar oxygen functionalities endow MXene with favorable interfacial compatibility toward the polymer matrix. The O 1s spectrum in Fig. 3(d) exhibits a dominant C-O peak located at ~532.5 eV, which is mainly attributed to Ti-OH moieties on the MXene surface. The coexistence of aforementioned chemical bonds greatly optimizes the interfacial adhesion between inorganic conductive fillers and organic WPU matrix, facilitating the construction of continuous and robust conductive networks throughout the composite.

The sensing mechanism of the d-MC/WPU strain sensor is illustrated in Fig. 4(a). In the initial state, a well-connected "MXene islands-MWCNTs bridges" network is formed within the WPU matrix, providing abundant in-plane and inter-plane electron transport pathways and resulting in the lowest electrical resistance. Under small strain, the slight separation of MXene sheets causes partial detachment from CNT bridges, leading to a gradual increase in resistance and a low gauge factor (GF). At large strain, significant stretching induces severe separation of MXene sheets and massive fracture of MWCNT-mediated inter-sheet pathways, resulting in a sharp increase in resistance and a high GF with excellent linearity. The Nyquist plots in Fig.4(b) reveal distinct differences in the electrical conductivity of the four materials. The pure MXene and MWCNTs samples exhibit the largest impedance values, indicating high charge transfer resistance and poor electrical conductivity due to severe sheet aggregation and

insufficient conductive pathways. In contrast, the MC composite shows a significantly reduced semicircle diameter, demonstrating the synergistic effect between MXene and MWCNTs in constructing a more continuous conductive network, thereby lowering the charge transfer resistance. Notably, the d-MC sample displays the smallest semicircle and the lowest overall impedance, confirming that the modification treatment of KH560 effectively optimizes the dispersion and interfacial contact between MXene and MWCNTs, establishing a highly efficient and low-resistance conductive network, which is crucial for achieving high-performance strain sensing.

The electronic band structure of the MXene/MWCNTs-KH560 composite calculated by DFT in Fig.4(c), reveals distinct metallic characteristics. Multiple energy bands directly cross the Fermi level (0 eV) without any band gap, confirming the excellent intrinsic electrical conductivity of the hybrid system. The dense distribution of energy bands near the Fermi level indicates a high density of states (DOS), which provides abundant free electrons for charge transport. Meanwhile, the dispersive nature of these bands suggests a low electron effective mass and high carrier mobility, which is favorable for achieving fast response and high sensitivity in strain sensing applications. Notably, the KH560 modification does not introduce localized defect states or disrupt the continuous conductive pathways, demonstrating that the silane coupling agent only optimizes the interfacial compatibility between MXene and CNTs while maintaining the high-performance electronic structure of the composite. The partial density of states (PDOS) of the MXene/CNTs-KH560 composite in Fig.4(d) reveals the electronic origin of its excellent conductivity. A finite total density of states is observed at the Fermi level (0 eV), confirming the metallic character of the system, consistent with the band structure results. Specifically, the states near the Fermi level are predominantly contributed by the d-orbitals, with additional contributions from p-orbitals, while the contribution of s-orbitals is negligible. This indicates that the electrical conductivity is mainly governed by the d-electrons of MXene, with complementary contributions from the p-electrons of CNTs, demonstrating effective electronic coupling and synergistic interaction between the two components. The overlap of p and d orbitals at the interface suggests that the KH560 modification optimizes the interfacial contact without disrupting the electronic transport pathways, thereby maintaining the high intrinsic conductivity of the composite.

The stress-strain curves in Fig. 4(e) reveal the mechanical behaviors of pristine WPU and the modified WPU composites with varied filler contents. Pure WPU shows

the weakest mechanical performance with an elongation at break of 1530% and tensile strength of 0.68 MPa, accompanied by the lowest initial modulus and deformation resistance, which indicates that pure WPU matrix cannot effectively transfer and dissipate stress during stretching, resulting in low toughness and mechanical strength. The introduction of low-content (0.5%) d-MC fillers preliminarily optimizes the mechanical properties, where d-$MC_{0.5}$/WPU presents slightly improved elongation at break (1580%), tensile strength (0.73 MPa) and stress response under equivalent strain, confirming the mild reinforcing effect of trace d-MC on the WPU matrix. When the d-MC loading increases to 1 wt%, d-MC_1/WPU achieves greatly enhanced ductility and tensile strength with elongation at break up to 2070% and tensile strength reaching 0.78 MPa, owing to the preliminary construction of internal stress transfer network that efficiently dissipates tensile energy. Further increasing the filler content to 2 wt% endows d-MC_2/WPU with the most optimal mechanical performance, with its elongation at break and tensile strength dramatically elevated to 2870% and 1.12 MPa respectively, since such appropriate doping dosage strengthens interfacial interaction, promotes molecular chain orientation and accelerates stress transmission, thus maintaining stable load-bearing capacity under large deformation. By contrast, excessive addition of d-MC leads to deteriorated comprehensive mechanical properties of d-MC_3/WPU, with decreased elongation at break of 2520% and tensile strength of 0.98 MPa. Consequently, the composite content of 2 wt% realizes synchronous enhancement in tensile strength and ductility, in which d-MC conductive fillers form favorable interfacial compatibility and synergistic effect with WPU substrate to build efficient stress transfer networks. In subsequent tests, d-MC_2/WPU composites were employed as the standard specimens. $_2$During tensile process, the interfacial interaction between fillers and matrix is capable of dissipating energy and delaying fracture, while the orientation and reconstruction of polymer molecular chains further improve load-bearing ability, thereby achieving the synergistic optimization of toughness and modulus and providing superior mechanical guarantee for flexible sensors applied in large-strain service scenarios.

The single cycle tensile stress-strain curves of the d-MC_2/WPU flexible sensor under maximum strains of 100%, 200% and 300% are presented in the Fig.4(f). All three curves exhibit typical elastic hysteresis behavior with well-defined closed loops, reflecting the energy dissipation induced by polymer chain slippage and dynamic filler-matrix interfacial interactions during stretching. The peak stress shows a significant

strain-dependent increase with the elevation of maximum strain: the peak stress reaches approximately 0.21 MPa at 100% strain, increases to about 0.32 MPa at 200% strain, and further rises to 0.4 MPa at 300% strain. This enhancement is attributed to the progressive orientation of WPU matrix chains and the gradual alignment and synergistic load-bearing of the filler network with increasing strain. Meanwhile, the area of the hysteresis loop expands remarkably with strain, indicating more active dynamic interactions and elevated energy dissipation at large deformations, which is directly correlated with the strain-dependent dynamic physical processes such as chain slippage and interfacial friction in flexible composites. Three curves exhibit smooth recovery behavior during unloading without obvious stress mutations or fracture, demonstrating excellent structural integrity and deformation reversibility of the material at different strain levels, which provides a reliable structural basis for its stable mechanical and electrical responses over a wide strain range.

The cyclic tensile stress-strain curves of the d-MC_2/WPU flexible sensor under 100% strain are presented in the Fig.4(g), where the blue curve corresponds to the first stretch-release cycle and the green curve cluster represents the 2nd to 20th cycles. In the first cycle, the material exhibits typical elastic hysteresis behavior, reaching a maximum stress of approximately 0.21 MPa at 100% strain. This phenomenon originates from the synergistic effect of segment slippage of the WPU matrix and the d-MC filler network, reflecting the abundant dynamic interactions within the material. After the initial cycle, the stress response stabilizes in subsequent cycles, accompanied by a significantly reduced and gradually stabilized hysteresis area, along with a high degree of curve overlap, demonstrating excellent mechanical repeatability and cyclic stability. These results indicate that the d-MC/WPU composites exhibit favorable structural reversibility during cyclic stretching, providing stable and reliable mechanical support for the flexible sensor under repeated deformation scenarios, which is an important guarantee for its high-performance and long-term stable sensing.

In Fig.5(a), the d-MC_2/WPU composite strain sensor exhibits distinct multi-stage sensing behavior across an ultra-wide strain range up to 2800%, with gauge factors (GF) of 0.11, 0.34, and 2.81 in the low (0-500%), medium (500-1500%), and high (1500-2800%) strain regions, respectively, and a high linear correlation coefficient ($R^2 = 0.994$) in the high-strain region, demonstrating excellent linearity and sensitivity under large deformation; this multi-gradient sensitivity, enabled by the synergistic “MXene islands-MWCNTs bridges” conductive network, allows the sensor to accommodate both subtle

physiological signal detection and large-scale human motion monitoring, while the ultra-high stretchability far exceeding that of conventional flexible sensors highlights the effectiveness of the WPU matrix and hybrid conductive fillers in constructing robust and high-performance strain sensing materials. The response and recovery times in Fig.5(b) are crucial indicators of sensor dynamic performance. The d-MC_2/WPU sensor shows a response time of 150 ms and a recovery time of 120 ms under 10% strain. The low viscoelasticity of WPU matrix and efficient charge transport of MXene/MWCNTs conductive network endow the sensor with fast response and recovery capabilities. Cycling stability is a critical guarantee for the practical application of sensors. Under tensile-releasing tests with 100% strain over 3000 cycles in Fig.5(c), the d-MC_2/WPU sensor exhibits highly stable resistance response and the variation profiles of $\Delta R/R_0$ at the initial and final stages of the cycles are similar.

Given the outstanding comprehensive performance of the d-MC_2/WPU flexible sensor, we further explored its application in human motion monitoring to evaluate its practical potential in physiological monitoring[34-35]. The sensor was attached to the wrist, elbow, thigh muscle, and knee joint to capture the bending motions of these body parts. As depicted in Fig. 6(a-d), during wrist flexion from 0° to 90°, the sensor delivered stable and repeatable $\Delta R/R_0$ signals, with the signal amplitude exhibiting a well-defined correlation with the bending angle. The signal waveforms remained highly consistent across different bending speeds, verifying its excellent dynamic response capability. Characteristic signals were also observed during elbow flexion-extension: when the elbow flexed, the sensor was stretched, increasing the spacing between conductive pathways and leading to a rapid rise in resistance, which reached a peak on the curve. When the elbow extended, the sensor recovered its deformation, the conductive pathways gradually reconstructed, and the resistance slowly decreased back to near the baseline. For knee joint motion monitoring, the peak $\Delta R/R_0$ reached approximately 160%-170%. Owing to the larger range of motion of the knee joint, the sensor was subjected to higher tensile strain, thus resulting in a greater resistance change rate. The variation trend of the thigh muscle signals was analogous to that of the knee joint.

4. Conclusion

In this work, flexible KH560-MXene/CNTs/WPU strain sensors are successfully fabricated using waterborne polyurethane as the flexible substrate, with MXene nanosheets and MWCNTs serving as synergistic conductive fillers. By optimizing the

mass ratio of MXene to MWCNTs, an efficiently interconnected conductive network with MXene as "conductive islands" and CNTs as "conductive bridges" is constructed. The resultant sensor delivers superior comprehensive sensing performances, including a high gauge factor (GF) of 2.81, an ultra-wide detectable strain range of 0-2800%, rapid response/recovery times of 150/120 ms, and outstanding cycling durability over 3000 loading-unloading cycles. First-principles calculations based on density functional theory (DFT) are performed to uncover the electronic configuration and strain-modulated mechanism at the MXene/MWCNTs heterointerfaces. Theoretical results verify evident interfacial charge transfer and orbital hybridization between MXene and MWCNTs. Moreover, the as-prepared sensor achieves real-time monitoring of large-amplitude human joint movements, subtle facial expressions and voice vibration recognition, demonstrating promising application prospects in wearable healthcare monitoring, sports motion analysis and human-machine interaction. This work provides both experimental foundations and theoretical guidelines for the rational design and performance optimization of high-performance flexible strain sensors.

CRediT authorship contribution statement

Xunlong Wang: Writing-original draft, Formal analysis, Data curation. Peng Shi: Methodology, Data curation. Zhaoliang Li: Funding acquisition. Shuyou Liu: Data curation. Qing Liu: Data curation. Ying Chen: Writing-review & editing.

Declaration of Competing Interest

The authors declare that they have no known competing financial interests or personal relationships that could have appeared to influence the work reported in this paper.

Data Availability Statement

Data will be made available upon request.

Conflict of Interest

The authors declared that they have no conflicts of interest to this work.

Acknowledgements

The authors gratefully acknowledge financial support from Advanced Materials-National Science and Technology Major Project (No. 2025ZD0620100) and Key R&D project of Shandong Province (No. 2025KJHZ034).

Reference

[1] O. A. Araromi, M. A. Graule, K. L. Dorsey, et al. Ultra-sensitive and resilient compliant strain gauges for soft machines. Nature, 2020, 587: 219-224.

[2] Bariya M, Shahpar Z, Park H, et al. Roll-to-roll gravure printed electrochemical sensors for wearable and medical devices. ACS Nano, 2018, 12(7): 6978-6987.
[3] Meng K, Xiao X, Wei W, et al. Wearable pressure sensors for pulse wave monitoring. Advanced Materials, 2022, 34(21): 2109357.
[4] Y. Wang, W. Qin, M. Yang, et al., High linearity, low hysteresis $Ti_3C_2T_x$ MXene/ AgNW/liquid metal self-healing strain sensor modulated by dynamic disulfide and hydrogen bonds, Advanced Functional Materials, 2023, 33 (37): 2301587.
[5] Li X, Li X, Liu T, et al. Wearable, washable, and highly sensitive piezoresistive pressure sensor based on a 3D sponge network for real-time monitoring human body activities. ACS Applied Materials & Interfaces, 2021, 13(39): 46848-46857.
[6] Pu J H, Zhao X, Zha X J, et al. Multilayer structured AgNW/WPU-MXene fiber strain sensors with ultrahigh sensitivity and a wide operating range for wearable monitoring and healthcare. Journal of Materials Chemistry A, 2019, 7(26): 15913-15923.
[7] Seyedin S, Uzun S, Levitt A, et al. MXene composite and coaxial fibers with high stretchability and conductivity for wearable strain sensing textiles. Advanced Functional Materials, 2020, 30(12): 1910504.
[8] Levitt A, Seyedin S, Zhang J, et al. Bath electrospinning of continuous and scalable multifunctional MXene-infiltrated nanoyarns. Small, 2020, 16(26): 2002158.
[9] Wang X, Tao Y, Pan S, et al. Biocompatible and breathable healthcare electronics with sensing performances and photothermal antibacterial effect for motion-detecting. NPJ Flexible Electronics, 2022, 6(1): 95.
[10] Tang Y, Yan J, Wang J, et al. MXene based flexible Janus nanofibrous membrane composite for unidirectional water transportation. Composites Science and Technology, 2023, 239: 110032.
[11] Lin H, Wang H, Yang Y, et al. Smart fabrics with liquid metal reinforced PU/CNT/MXene multilayer structures for constructing multifunctional sensors and wearable electronics. Journal of Materials Chemistry A, 2024, 12(44): 30872-30884.
[12] Yan K, Chen H, Li X, et al. Scalable and multifunctional polyurethane/MXene/carbon nanotube-based fabric sensor toward baby healthcare. ACS Applied Materials & Interfaces, 2024, 16(4): 5196-5207.
[13] Yu C, Wang Y, Qiu X, et al. Ultrarobust self-healing elastomers with hydrogen bonding connected MXene network for actuator applications. Chemical Engineering Journal, 2023, 475: 146079.

[14] X. Liang, F. Dai, et al., Epoxy nanocomposites with reduced graphene oxide-constructed three-dimensional networks of single wall carbon nanotube for enhanced thermal management capability with low filler loading, ACS Appl. Mater. Interfaces, 2019,12: 3051-3058.
[15] Wu G, Yang Z, Zhang Z, et al. High performance stretchable fibrous supercapacitors and flexible strain sensors based on CNTs/MXene-TPU hybrid fibers. Electrochimica Acta, 2021, 395: 139141.
[16] Yang Z, Li H, Zhang S, et al. Superhydrophobic MXene@ carboxylated carbon nanotubes/carboxymethyl chitosan aerogel for piezoresistive pressure sensor. Chemical Engineering Journal, 2021, 425: 130462.
[17] Ma X, Tu X, Gao F, et al. Hierarchical porous MXene/amino carbon nanotubes-based molecular imprinting sensor for highly sensitive and selective sensing of fisetin. Sensors and Actuators B: Chemical, 2020, 309: 127815.
[18] Zhao X, Lin X, Yao Z, et al. Plant growth monitoring, prediction, and self-regulation utilizing MXene/CNTs/TPU flexible strain sensors integrated with deep learning algorithms and soft actuators. Science China Materials, 2025, 68(10): 3715-3727.
[19] Jiang S, Wang Z, Li S, et al. High-Performance Pressure and Temperature Dual-Mode Sensor Based on Thermoelectric Aerogels for Multimodal Intellectual Panel Application. Advanced Materials Technologies, 2025, 10(11): 2401891.
[20] Sun B, Xu G, Yang Z, et al. Dual-mode temperature monitoring using high-performance flexible thermocouple sensors based on PEDOT: PSS/CNTs and MXene/Bi_2Se_3. Microsystems & Nanoengineering, 2025, 11(1): 31.
[21] Zhang D, Yin R, Zheng Y, et al. Multifunctional MXene/CNTs based flexible electronic textile with excellent strain sensing, electromagnetic interference shielding and Joule heating performances. Chemical Engineering Journal, 2022, 438: 135587.
[22] Zhang R, Lin J, He T, et al. High-performance piezoresistive sensors based on transfer-free large-area PdSe2 films for human motion and health care monitoring. InfoMat, 2024, 6(1): e12484.
[23] Wu H, Wang C, Liu L, et al. Bioinspired stretchable strain sensor with high linearity and super hydrophobicity for underwater applications. Advanced Functional Materials, 2025, 35(3): 2413552.

[24] Ma Z, Ma K, Lu S, et al. Flexible Ti3C2Tx MXene/ink human wearable strain sensors with high sensitivity and a wide sensing range. Sensors and Actuators A: Physical, 2020, 315: 112304.
[25] Huang Y, Huang H, Guo Y, et al. Thermoplastic Polyurethane/MXene Nanosheet/SiO2 Nanoparticle Composites for Superhydrophobic Surfaces and Wearable Strain Sensors. ACS Applied Nano Materials, 2025, 8(19): 9849-9859.
[26] Xu H, Jiang X, Yang K, et al. Conductive and eco-friendly gluten/MXene composite organohydrogels for flexible, adhesive, and low-temperature tolerant epidermal strain sensors. Colloids and Surfaces A: Physicochemical and Engineering Aspects, 2022, 636: 128182.
[27] Herber M, Hill E H. Optically-directed bubble printing of MXenes on flexible substrates toward MXene-enabled wearable electronics and strain sensors. Nano Letters, 2025, 25(18): 7258-7265.
[28] Kumar A, Kumar R K R, Shaikh M O, et al. Wearable strain sensor utilizing the synergistic effect of $Ti_3C_2T_x$ MXene/AgNW nanohybrid for point-of-care respiratory monitoring. Materials Today Chemistry, 2024, 37: 102024.
[29] Jiang C, Xie W, Wu D. Balancing the overall performance of poly (vinyl alcohol)/MXene composite organohydrogels for flexible strain sensors. ACS Applied Polymer Materials, 2022, 5(1): 370-380.
[30] Shi X, Wang H, Xie X, et al. Bioinspired ultrasensitive and stretchable MXene-based strain sensor via nacre-mimetic microscale “brick-and-mortar” architecture. ACS nano, 2018, 13(1): 649-659.
[31] Zhu D, Duan S, Liu J, et al. A double-crack structure for bionic wearable strain sensors with ultra-high sensitivity and a wide sensing range. Nanoscale, 2024, 16(10): 5409-5420.
[32] Zhang J, Zhang S. A highly stretchable strain sensor fabricated based on freeze-thaw polymerized MXenes-doped hydrogel for monitoring human joint movement. Vacuum, 2025, 234:114738.
[33] Wang B, Qiu Z, Wei Y, et al. Nanofiber yarn strain sensor with interpenetrating 3D MXene network via conjugated electrospinning and deep deposition. Materials Today Physics, 2026,47:102086.
[34] Hu L, Xie Y, Gao S, et al. Strain-induced orientation facilitates the fabrication of highly stretchable and tough xylan-based hydrogel for strain sensors. Carbohydrate Polymers, 2023, 312: 120827.

[35] Zhang S, Xiao Y, Chen H, et al. Flexible triboelectric tactile sensor based on a robust MXene/leather film for human-machine interaction. ACS Applied Materials & Interfaces, 2023, 15(10): 13802-13812.

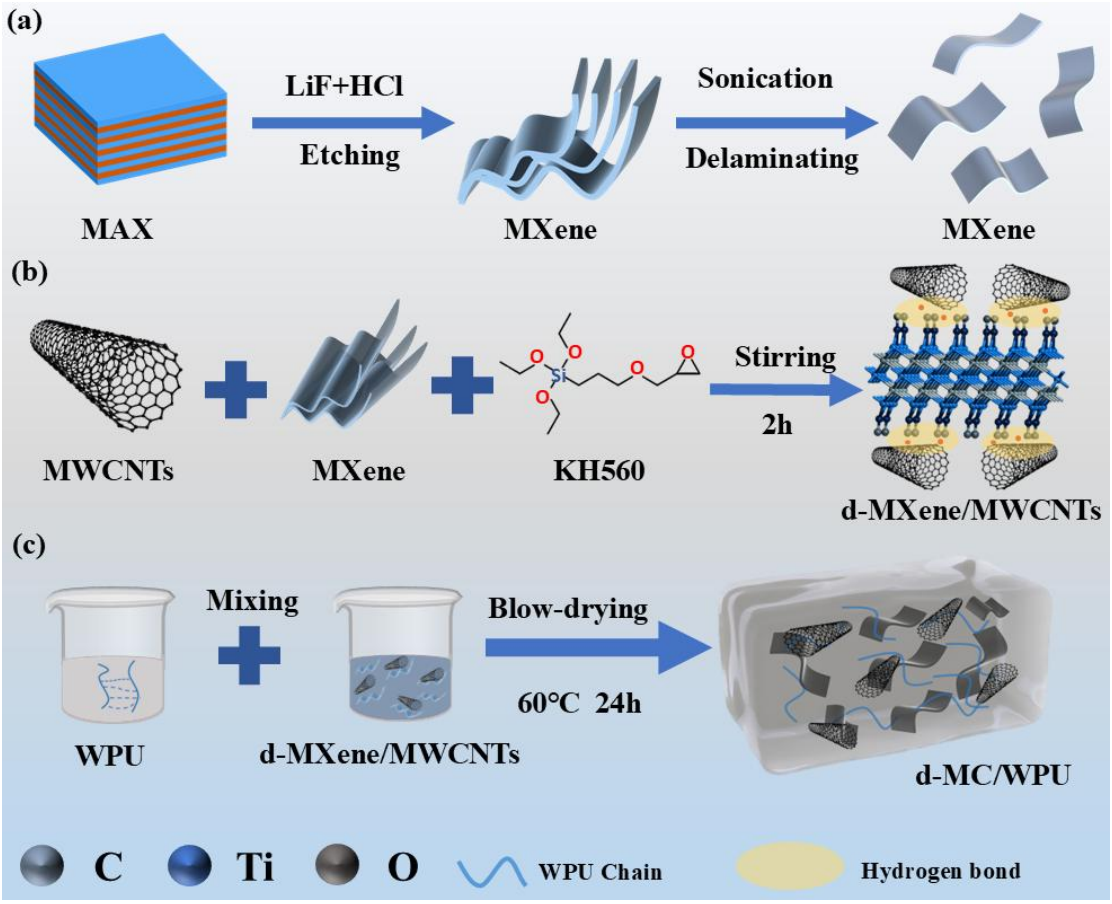


Fig.1. Preparation processes of different materials: (a) Single-layer MXene, (b) d-MC, (c) d-MC_x/WPU composite.

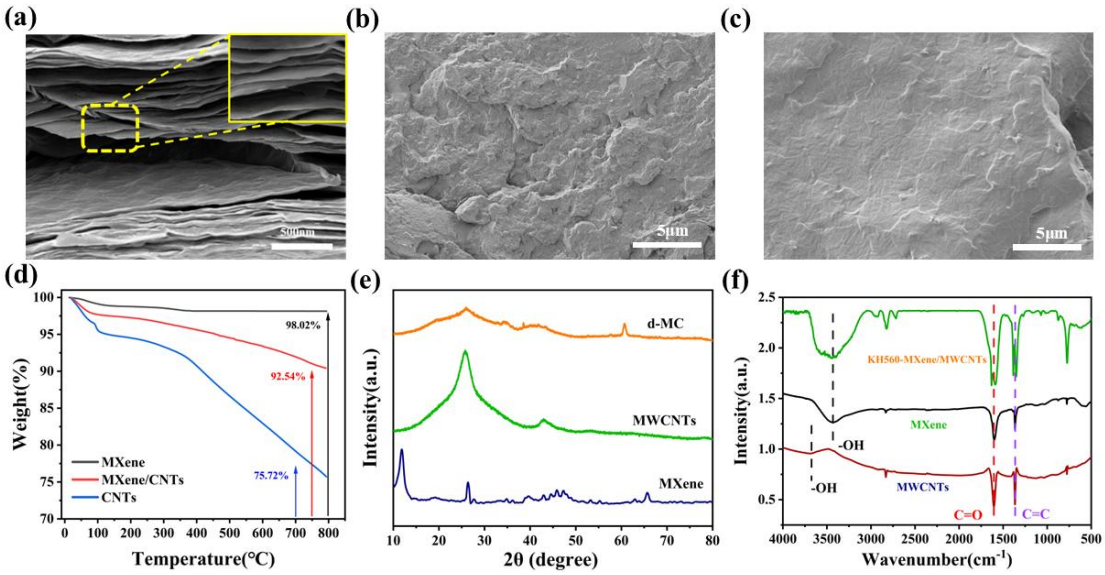


Fig.2. (a) SEM image of pristine single-layer MXene, (b) Cross-sectional SEM micrograph of $MC_{0.5}$/WPU composite film, (c) Cross-sectional SEM micrograph of modified d-MC_2/WPU composite film, (d) TGA curves of pristine MXene, MXene/MWCNTs and pure MWCNTs, (e) XRD patterns of MXene, MWCNTs and d-MC hybrid fillers (f) FTIR spectra of MXene, MWCNTs and d-MC composite fillers**.**

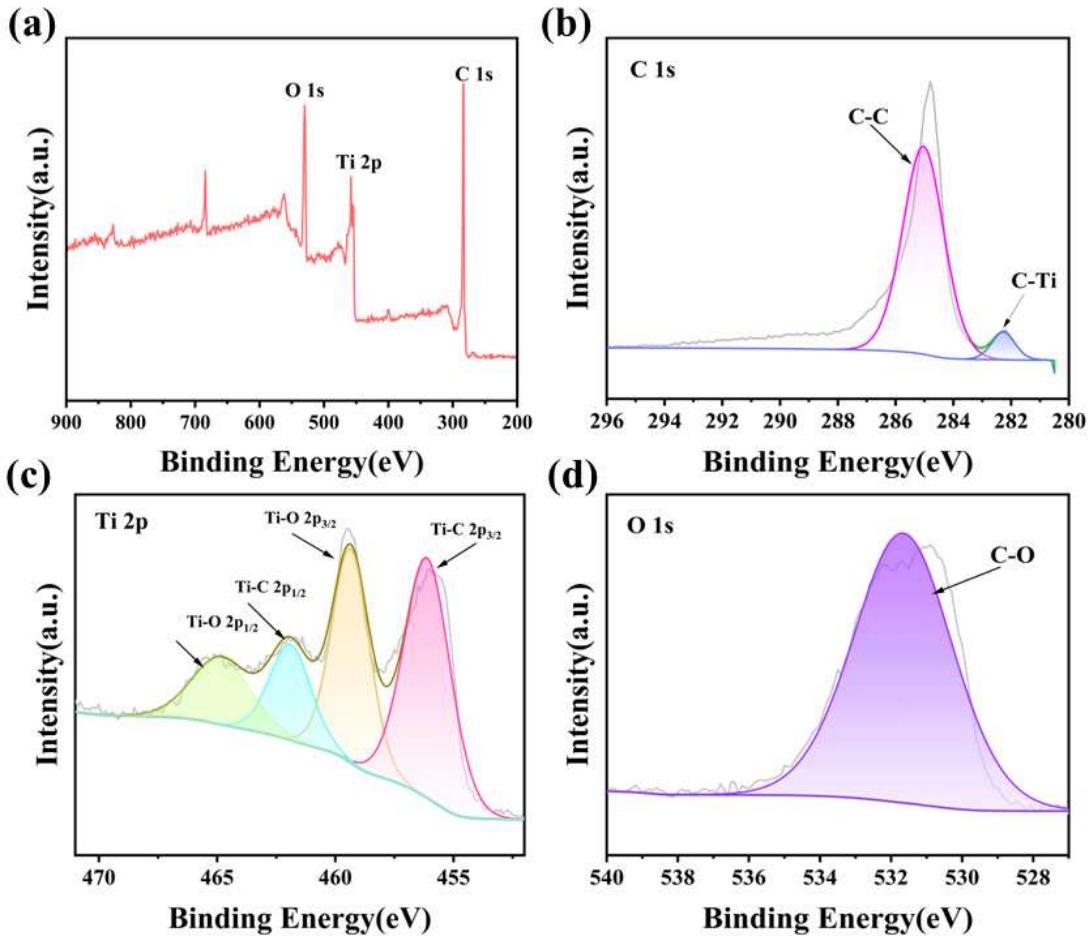


Fig.3. High-resolution XPS spectra of (a)d-MXene/MWCNTs, (b) C1s spectra of d-MXene/MWCNTs, (c) O1s spectra of d-MXene/MWCNTs, (d) Ti2p spectra of d-MXene/MWCNTs.

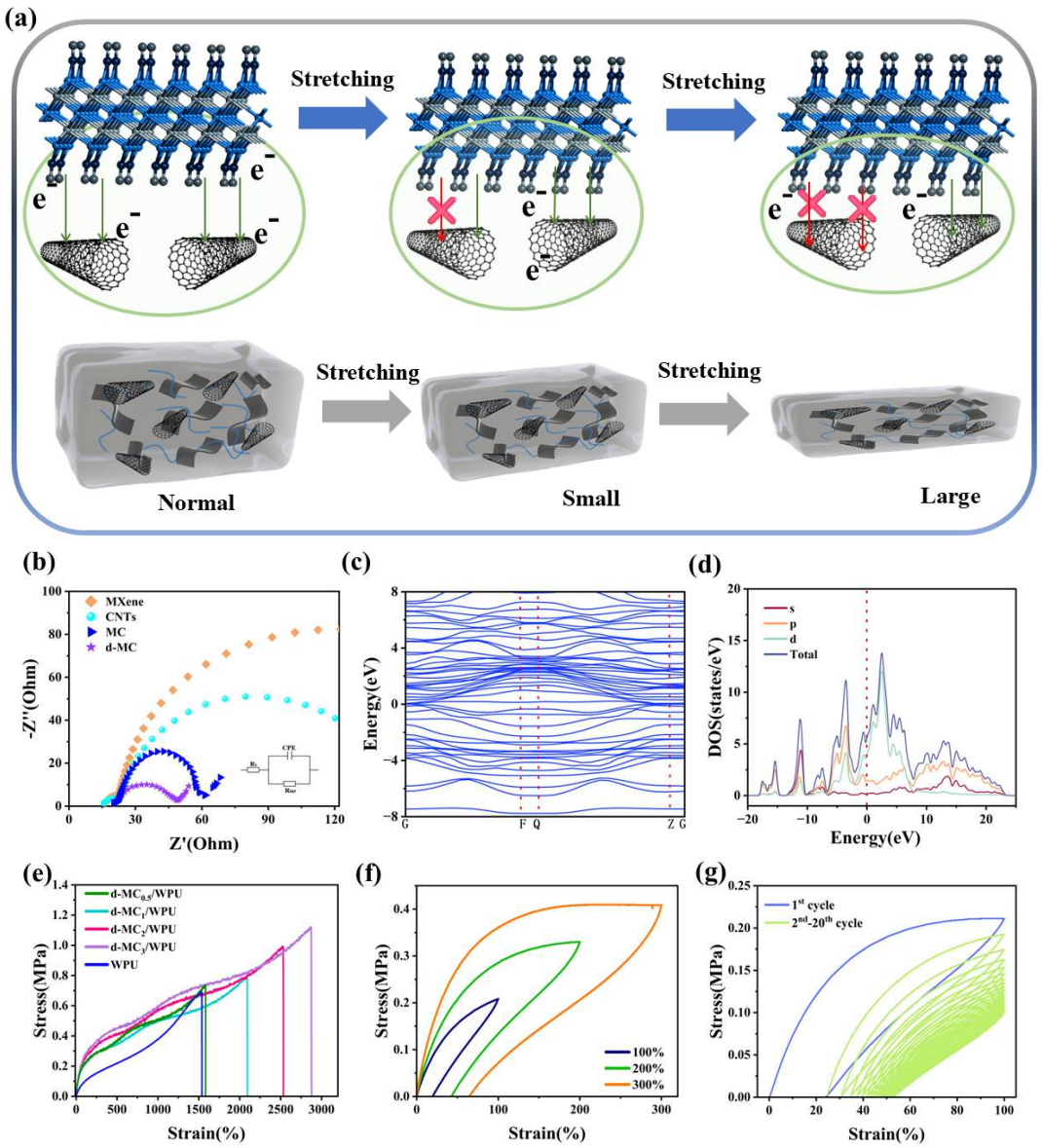


Fig.4. (a) Schematic illustration of the mechanism of d-MC/WPU flexible sensor ,(b) Impedance plots of MXene, MWCNTs, MC and d-MC, (c) Band structure of d-MC, (d) Schematic density of states of d-MC, (e) Mechanical properties of pure WPU and d-MC/WPU composites with different filler contents, (f) Single cycle curves under strains of 100%, 200% and 300%, (g) Stress-strain curves for 1-20 tensile cycles at 100% strain.

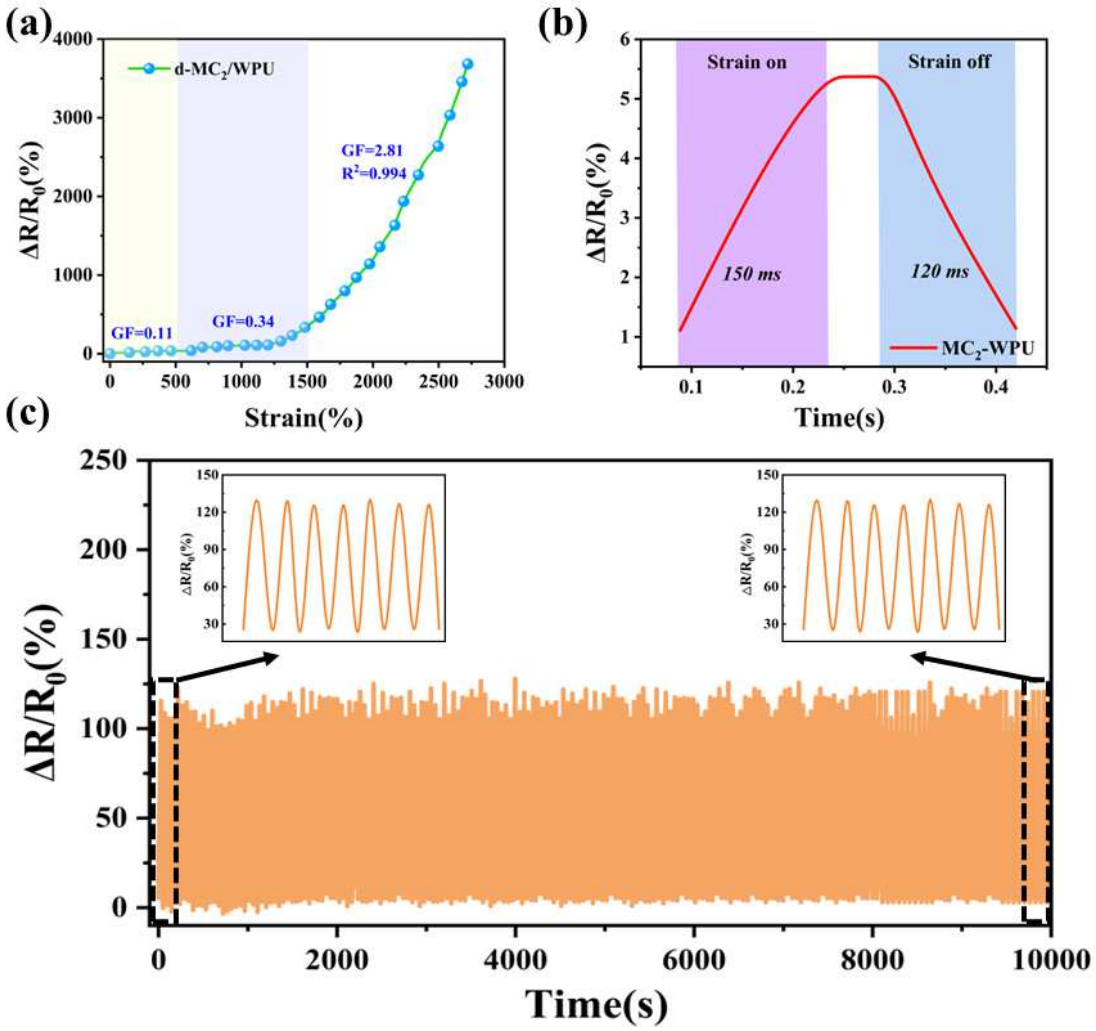


Fig.5. (a) Gauge factor of d-MC_2/WPU, (b) Response and recovery time under 10% tensile strain, (c) Variation curves of resistance response during 3000 cycles.

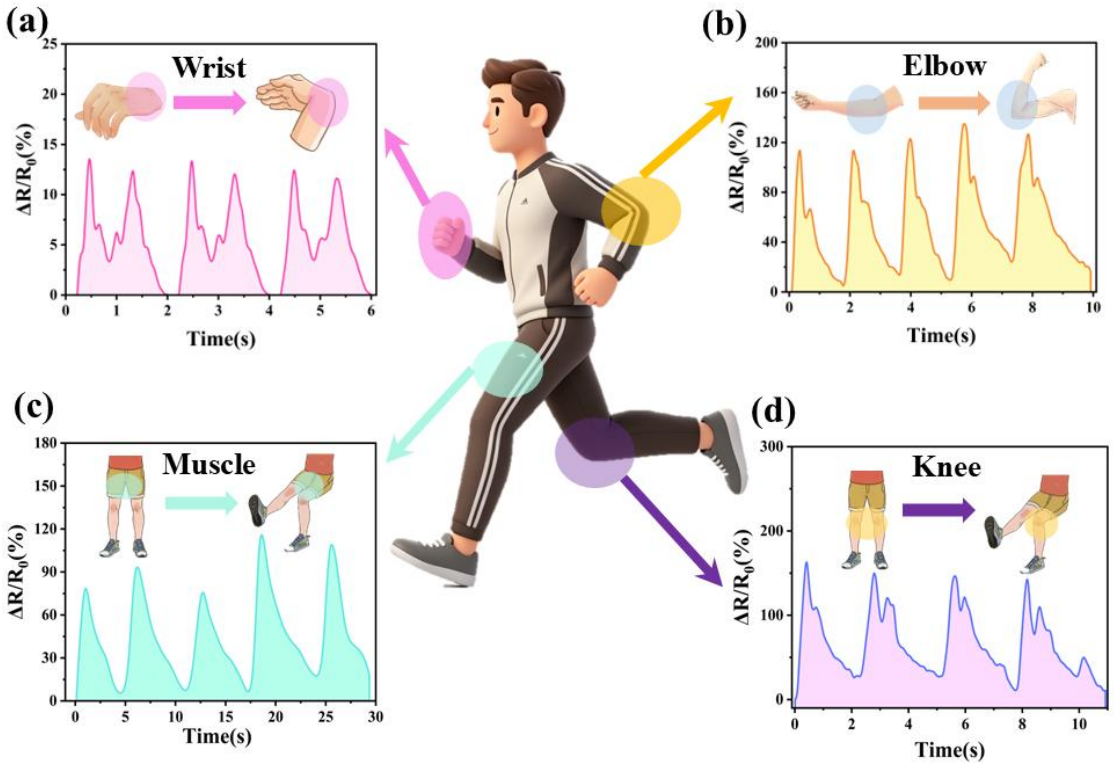


Fig.6. Schematic diagram of human body motion posture monitoring (a) Wrist flexion, (b) Elbow flexion, (c) Muscle activity, (d) Knee joint flexion.